Astronomy & Astrophysics manuscript no. Huang˙M71
December 6, 2009
© ESO 2009

arXiv:0912.1148v1 [astro-ph.SR] 6 Dec 2009

Study of HST counterparts to Chandra X-ray sources in the Globular Cluster M71

R. H. H. Huang[1], W. Becker[1], P. D. Edmonds[2], R. F. Elsner[3] C. O. Heinke[4], and B. C. Hsieh[5]

[1] Max-Planck-Institut für extraterrestrische Physik, Giessenbachstrasse 1, 85748 Garching, Germany
[2] Harvard-Smithsonian Center for Astrophysics, Cambridge, MA 02138, USA
[3] NASA Marshall Space Flight Center, Huntsville, AL 35812, USA
[4] Department of Physics, University of Alberta, Edmonton, Alberta, Canada
[5] Institute of Astronomy and Astrophysics, Academia Sinica, Taipei 10617, Taiwan

Preprint online version: December 6, 2009

ABSTRACT

Aims. We report on archival Hubble Space Telescope (HST) observations of the globular cluster M71 (NGC 6838).
Methods. These observations, covering the core of the globular cluster, were performed by the Advanced Camera for Surveys (ACS) and the Wide Field Planetary Camera 2 (WFPC2). Inside the half-mass radius (r_h = 1.′65) of M71, we find 33 candidate optical counterparts to 25 out of 29 Chandra X-ray sources while outside the half-mass radius, 6 possible optical counterparts to 4 X-ray sources are found.
Results. Based on the X-ray and optical properties of the identifications, we find 1 certain and 7 candidate cataclysmic variables (CVs). We also classify 2 and 12 X-ray sources as certain and potential chromospherically active binaries (ABs), respectively. The only star in the error circle of the known millisecond pulsar (MSP) is inconsistent with being the optical counterpart.
Conclusions. The number of X-ray faint sources with $L_X > 4\times10^{30}$ ergs s^{-1} (0.5–6.0 keV) found in M71 is higher than extrapolations from other clusters on the basis of either collision frequency or mass. Since the core density of M71 is relatively low, we suggest that those CVs and ABs are primordial in origin.

Key words. globular clusters: individual (M71, NGC 6838)

1. Introduction

There are 158 Galactic globular clusters (GGCs) found in the halo of our galaxy and typically contain 10^4 – 10^7 stars. They are very old and dense star systems and tightly bound by gravity, which gives them their spherical shapes and relative high stellar density toward the center. The dense stellar environment in globular clusters triggers various dynamical interactions, ie. exchanges in encounters with binaries, direct collisions, destruction of binaries, and tidal capture. These dynamical interactions not only can change the evolution of individual stars, but also can produce tight binary systems (see, e.g., Ashman & Zepf 1998; Verbunt & Lewin 2004, for review).

One of the most powerful ways to probe the binary content of globular clusters is by studying the X-ray source population. In the early 1970s, X-ray sources with luminosity greater than 10^{36} ergs s^{-1} were first detected by using the Uhuru and OSO-7 Observatories. Following the Einstein and ROSAT era, the number of faint X-ray sources ($L_X < 10^{34.5}$ ergs s^{-1}) was dramatically increased. Those bright X-ray sources have been identified with low-mass X-ray binaries (LMXBs; Grindlay et al. 1984) while the identification of the weaker sources remained limited due to low photon statistics and insufficient spatial resolution. The launch of the Chandra X-ray Observatory ushered in a new age of studying the crowded centers of Galactic globular clusters with a far greater sensitivity and resolving power than ever before (e.g., Grindlay et al. 2001a,b). With the aid of the Hubble Space Telescope (HST), many of these faint X-ray sources were identified as quiescent low-mass X-ray binaries (qLMXBs; in which a neutron star accretes matter from its companion at a low rate), cataclysmic variables (CVs; in which a white dwarf accretes from its low-mass companion), and millisecond pulsars (MSPs), as well as chromospherically active binaries (ABs; e.g., RS CVn and BY Dra systems) (e.g., Grindlay et al. 2001b; Pooley et al. 2002; Edmonds et al. 2003a,b; Heinke et al. 2005; Bassa et al. 2004; Kong et al. 2006; Lugger et al. 2007; Bassa et al. 2008).

The globular cluster M71 (NGC 6838) lies close to the Galactic plane with Galactic longitude l = 56.°74 and latitude b = −4.°56. Similarly to 47 Tuc, it is a fairly metal-rich globular cluster with metallicity of [Fe/H] = −0.73. Due to its relatively small distance (d ∼ 4 kpc) to Earth and low central luminosity density ($\rho_c = 10^{3.05}\,L_\odot/pc^3$), M71 is a good target for both optical and X-ray observations. The core, half-mass, and tidal radii are r_c = 0.′63, r_h = 1.′65, and r_t =8.′96, respectively. M71 shows no evidence for core collapse. Its moderate optical reddening E_{B-V} = 0.25 may be converted into a nominal X-ray absorption column of $N_H = 1.39\times10^{21}$cm^{-2} (Predehl & Schmitt 1995). The aforementioned parameters related to M71 were obtained from Harris (1996, updated 2003[1]).

In this work we report on archival Chandra and HST observations of the globular cluster M71. We have obtained a 52.4-kilosecond Chandra observation of M71 taken with the Advanced CCD Imaging Spectrometer (ACIS), reaching the limiting X-ray luminosities of 1.5×10^{30} ergs s^{-1} and 7.9×10^{29} ergs s^{-1} in the energy ranges of 0.3–8.0 and 0.5–2.5 keV, re-

Send offprint requests to: R. H. H. Huang (rhuang@mpe.mpg.de)

[1] http://physwww.mcmaster.ca/ harris/Databases.html

spectively. In Elsner et al. (2008), we reported the identification of 29 X-ray sources within the cluster half-mass radius, including the known millisecond pulsar PSR J1953+1846A (M71A), and their X-ray properties, and found that 18 ± 6 of these 29 sources are likely to be associated with M71 from a radial distribution analysis. The present paper extends our study of the X-ray sources in M71 by using archival HST data to identify optical counterparts to the majority of M71's X-ray sources, improving our understanding of their nature.

In §2 we discuss the Chandra X-ray observations and spectral analysis. HST observations, data reduction and analysis are described in §3. In §4 we present the source identification. A discussion and comparison with other globular clusters is given in §5.

2. X-ray Observations

Elsner et al. (2008) described the Chandra X-ray observations of M71. We here note some relevant information for our analysis and extend the spectral fitting in this paper to test alternative models besides the power-laws considered by Elsner et al. (2008). Only seven of the 29 detected X-ray sources have sufficient counts (six sources with at least 50 source counts and one known MSP with 37.5 source counts[2]) to warrant a detailed spectral analysis. We used the CIAO tool *dmextract* to extract spectra of the brighter sources and the source-free background regions near to those sources. Response files were constructed by using the CIAO tool *mkacisrmf* and *mkarf*. The extracted spectra were binned with at least 5 source counts per bin. Background-subtracted spectral modeling was performed with XSPEC using data in the energy band 0.3–8.0 keV. To characterize the spectra of these sources, we fitted each of the 7 brightest X-ray sources with several different models (i.e., power-law (PL), thermal bremsstrahlung (TB), and blackbody (BB)) by using Cash (1979) statistics. Assuming all the X-ray sources within the half-mass radius are associated with the globular cluster M71, we fixed the hydrogen column density at the value of $N_{\rm H} = 1.39 \times 10^{21}$ cm^{-2} from optical extinction to attempt spectral fitting.

In Table 1, column 1 shows the Chandra source name given in Elsner et al. (2008), and column 2 lists the spectral model we used (we omitted the models that could not provide any physically acceptable description of the observed spectra). Column 3 gives the minimum number of counts used to group the spectral data for fitting, column 4 shows the best-fit photon index (Γ) or the temperature (keV), column 5-6 gives the C-statistic and the number of PHA[3] bins, and the last column lists the unabsorbed X-ray flux in units of 10^{-14} ergs s^{-1} cm^{-2} in the energy bands 0.3–8.0 and 0.5–2.5 keV.

The X-ray spectra discussed here can help us to classify the faint X-ray sources. The brightest X-ray sources with $L_{\rm X} \geq 10^{32}$ ergs s^{-1} in the energy band 0.5–2.5 keV and soft spectra ($f_{0.5-2.0\ \rm keV}/f_{2.0-6.0\ \rm keV} \geq 1$) are mostly quiescent low-mass X-ray binaries (qLMXBs; Verbunt et al. 2008). None of the X-ray sources in our sample shows this characteristic, and we conclude that M71 does not contain this kind of binary systems. Cataclysmic variables (CVs) usually have hard spectra (power-law photon indices $\Gamma < 2$) and their X-ray luminosities are typically between a few 10^{30} and a few 10^{32} ergs s^{-1}. Most faint ($L_{\rm X} < 3 \times 10^{31}$ ergs s^{-1}) sources with soft spectra belong to chromospherically active binaries (ABs; Verbunt et al. 2008). Looking at the brightest seven X-ray sources within the half-mass radius, we see that three have soft spectra ($\Gamma > 2$), three have hard spectra ($\Gamma < 2$), and one (s20) is borderline, with $\Gamma \sim 2$. These spectra suggest that s05, s08, and s29 might be CVs, AGN, or MSPs, while the softer spectra of s02, s15, s19 and s20 may indicate that these are ABs. Definitive classifications require optical identification, which we turn to now.

3. Optical Observations

Two fields located inside the half-mass radius of the globular cluster M71 were observed with the Wide Field and Planetary Camera 2 (WFPC2) on board the Hubble Space Telescope (HST) in 2000 and 2006. An image of the observations is shown in Figure 1. For these observations, the PC camera was centered on the cluster center and the F336W (similar to U, hence U_{336} hereafter), F439W (B_{439}), and F555W (V_{555}) filters were used. Exposure times were 800 sec in F336W (GO10524) and 240 sec in F439W (GO8118). Two exposure times correspond to the F555W filter are 80 sec and 63 sec for GO10524 and GO8118, respectively. GO10524 also contains F255W images which did not go deep enough to identify our targets. To estimate whether the nondetections may be meaningful, we used Ferraro et al. (2000) to estimate that CVs may be up to 3 magnitudes brighter (absolute magnitude) in F255W than V. Using Seaton (1979), we estimate the extinction $A_{255} = 7.0$ for M71, and thus any CVs would be observed to be at least 3.2 magnitudes fainter in F255W than V. Using the WFPC2 exposure time calculator (ETC), we estimate that the brightest CV candidate in our WFPC2 field, s29, could attain a signal-to-noise ratio (SNR) of 1.4 in the F255W data if it showed the maximum F255W/V excess, which many of Ferraro et al.'s UV-selected objects do not. Therefore we did not discuss the F255W data further in this paper. The 5-σ limiting magnitudes of U_{336}, B_{439}, and V_{555} for point sources are 21.09, 20.87, and 21.87, respectively. M71 was also observed with the HST Advanced Camera for Surveys (ACS). The observations (GO10775) consist of F606W (V_{606}) and F814W (I_{814}) images covering the entire half-mass radius of the cluster (see Fig. 1). The exposure times for the F606W and F814W filters were 304 and 324 sec with 5-σ limiting magnitudes of $V_{606} = 25.17$ and $I_{814} = 23.91$ for point sources. We note that the median value of the point sources with the signal to noise ratio S/N ~ 5 is used to define the 5-sigma limiting magnitude.

This section outlines the data reduction, photometry, and astrometry of the HST/WFPC2 and ACS images.

3.1. Data Reduction and Photometry

The HST/WFPC2 data obtained from the ESO archive were processed through the WFPC2 Associations Science Products Pipeline[4]. For each filter, single exposures were calibrated, including full bias subtraction and flat-fielding, and combined together in order to remove the cosmic-ray events and correct the geometrical distortions [5]. We also downloaded the archival HST/ACS drizzled images. Those images were combined from two Wide Field Channel (WFC) images and calibrated with MultiDrizzle package (Koekemoer et al. 2002), which corrected for geometric distortion and performed cosmic ray rejection.

[2] The number of source counts is a result of modelling the background and the PSF, and represents a background subtracted expectation value for the source counts within the detect cell.

[3] PHA: Pulse Height Analysis

[4] See http://archive.eso.org/archive/hst/wfpc2_asn/

[5] see http://archive.stsci.edu/hst/wfpc2/pipeline.html

Table 1. Spectral fits of the X-ray sources with source counts $C_{0.3-8.0\ \mathrm{keV}} \geq 50$

X-ray Source	Model	Grouping[a]	Γ/kT	C-statistic/bins	$f_{0.3-8.0}(f_{0.5-2.5})$[b]
s02	PL	8	3.08±0.3	12.11/9	1.49(0.74)
	TB	8	0.62±0.1	10.99/9	1.26(0.82)
s05	PL	30	1.55±0.1	8.20/9	5.67(2.25)
	TB	30	$9.96^{+9.2}_{-3.0}$	10.33/9	5.48(2.23)
	BB	30	$0.69^{+0.04}_{-0.03}$	59.72/9	2.63(0.91)
s08	PL	5	1.70±0.5	2.56/6	0.74(0.32)
	TB	5	0.53	20.18/6	0.67(0.45)
s15	PL	5	2.57±0.3	9.34/11	1.18(0.63)
	TB	5	$1.31^{+0.5}_{-0.3}$	8.23/11	0.84(0.57)
s19	PL	5	2.61±0.4	1.19/9	1.14(0.60)
	TB	5	$1.23^{+0.7}_{-0.3}$	2.77/9	0.80(0.55)
s20	PL	8	1.92±0.4	9.52/9	1.71(0.83)
	TB	8	$1.90^{+2.1}_{-0.7}$	8.58/9	1.40(0.89)
	BB	8	$0.35^{+0.04}_{-0.03}$	0.84/7	0.83(0.72)
s29	PL	5	1.29±0.4	4.94/8	1.12(0.36)

[a] Minimum number of counts used to group the spectral data for fitting in XSPEC.
[b] Unabsorbed X-ray flux in units of 10^{-14} ergs s^{-1} cm^{-2}; energy bands are 0.3–8.0 (0.5–2.5) keV.

Although M71 is a globular cluster, its stellar surface density is not as dense as that of a typical globular cluster. Even in the central region of M71, the average distance between stars is around 2″, which is about 10 times larger than the typical FWHMs of WFPC2 and ACS cameras. Therefore, a simple aperture photometry method with the aperture correction is applicable to our data. We tested the flux measurement using several different psf-fitting photometry methods and the simple aperture photometry. We found that aperture photometry method had better signal-to-noise ratio and less magnitude error. Therefore, we decided to use aperture photometry to measure the fluxes of our data.

For the data taken with WFPC2, we basically followed the instruction of aperture photometry described in Holtzman et al. (1995). To deal with the PSF variances within each chip and between chips, we further separated the images into 4 and 9 equal-size regions for the PC and WF chips, respectively, and performed the aperture photometry with aperture correction for each separated regions individually. We used an aperture with the size of 0.″5 in radius to measure fluxes, for all the objects with 3 σ detection found using the IRAF *daofind* task. We note that only less than 1% objects in each chip with separation of $\leq$ 0.″5 to their neighbors, so that using an aperture with the size of 0.″5 does not suffer from the PSF overlapping problem. The local sky values were measured using an inner sky annulus of 4 arcsecs with a width of 2 arcsecs, and the aperture correction value was calculated using the averages of the differences between the magnitudes measured using apertures with sizes of 0.″5 and 4″ in radius for 4 to 5 isolated stars in each separated region. The aperture correction value is 0.11±0.02 mag, which is consistent with the value shown in Holtzman et al. (1995). The final output magnitudes, in the VEGAMAG system, were corrected for the appropriate zeropoints based upon the sensitivity information in each header and the charge transfer efficiency effect (Dolphin 2000).

For the data taken with ACS, we performed the aperture photometry based on the method described in Sirianni et al. (2005). The method is very similar to what we did for WFPC2. We also separated the ACS drizzled images into 9 equal-size regions to deal with the PSF variances. We used an aperture size of 0.″5 in radius to measure the fluxes with sky annulus from 4 arcsecs to 6 arcsecs. The aperture correction value is 0.08±0.01, which agrees with the values shown in Sirianni et al. (2005). However, several optical counterparts, e.g., s08, s19, suffer from the PSF overlapping problem since the distances between them and their neighbors are $\lesssim$ 1.″0. In order to measure accurate fluxes for these counterparts, we first subtracted their neighbors by using the PSF generated from isolated stars which are close to the counterparts, and then performed the aperture photometry on these sources. By doing this, we can minimize the photometric effect from the PSF wings of neighbors.

Comparing with the photometry of M71 kindly provided by Anderson et al. (2008) for the ACS images and reported by Piotto et al. (2002) for the WFPC2 B-band and V-band images, their results are consistent with what we have obtained by using aperture photometry, but have the main sequence and the giant branch with less noise. We therefore used their photometry in our study. In addition, for those possible optical counterparts undetected in their photometry, we used our own results for the magnitudes which have been corrected for the appropriate zeropoint.

The most informative of these diagrams are shown in Fig. 2, on which all stars located within the 95% confidence error circles (see Section 2 and Table 1 of Elsner et al. 2008) of the Chandra source positions are indicated by red squares. Numbers have been assigned to all candidate counterparts corresponding to the 's' designation given in Elsner et al. (2008), with 'a', 'b', or 'c' appended if multiple potential optical counterparts exist.

3.2. Astrometry

To search for optical counterparts to the Chandra X-ray sources we aim to place both the X-ray and the optical frames onto the International Celestial Reference System (ICRS). We use this approach to improve the absolute pointing accuracy of Chandra and HST, 0.″6 and 1.″0 (1σ) respectively (Aldcroft et al. 2000; Heyer et al. 2004).

For the X-ray sources, the positions listed in Elsner et al. (2008) are already on the ICRS. In this paper, we aim to tie the HST pointing to the ICRS by finding matches between stars appearing on HST images and stars with accurate positions in the Two Micron All Sky Survey (2MASS) Point Source Catalog (Skrutskie et al. 2006). On the basis of the HST pointing information contained in each image header, we used the

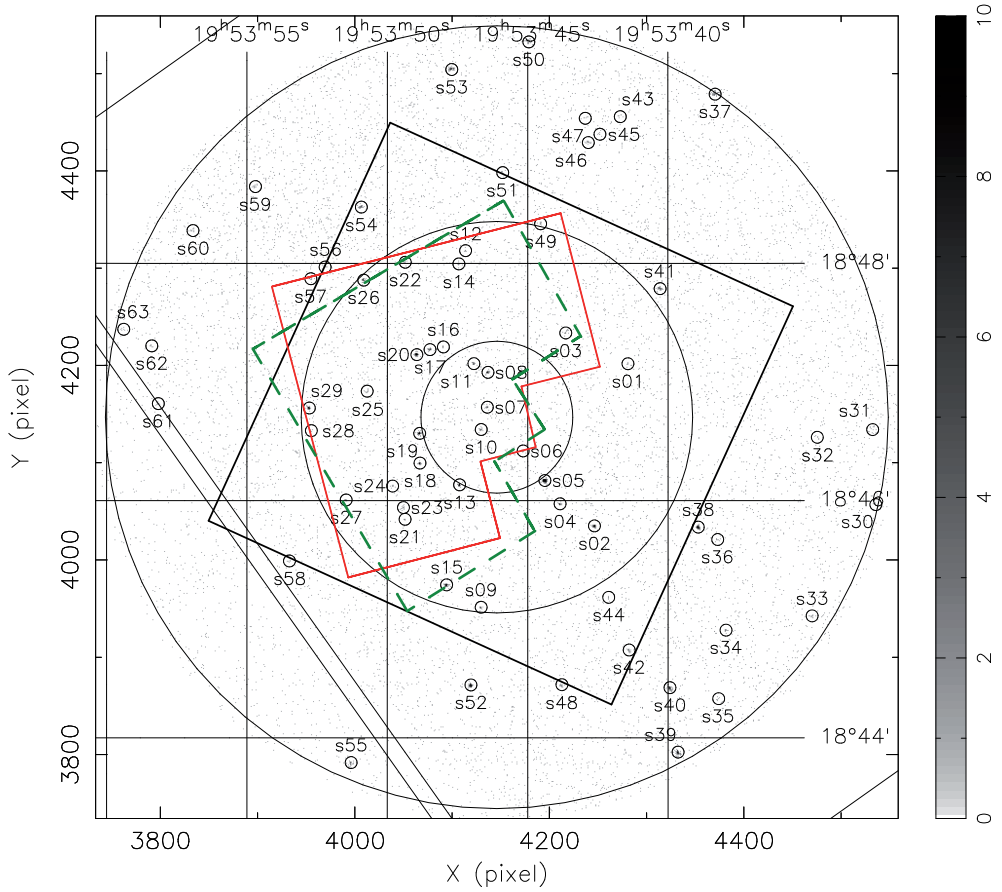

Fig. 1. Chandra ACIS-S3 image of the globular cluster M71 within the energy range of 0.3 – 8.0 keV. The large circles are centered on the nominal center of the cluster and have radii r_c (inner circle), r_h (middle circle), and $2r_h$ (outer circles). The small circles show the positions of the 63 X-ray sources within $r_{M71} \leq 2r_h$ (Elsner et al. 2008). Straight lines mark the nominal boundaries of the ACIS-S3 and ACIS-S2 CCDs, with most of the figure falling on S3 and the lower left hand portion on S2. The field of view of the HST ACS (GO10775) marked by the black square covers the entire half-mass radius. The green (dashed) and red (solid) polygons are the field of view of the HST WFPC2 for GO10524 and GO8118, respectively.

WCSTools/*imwcs*[6] task on each corrected image to do the cross-correlation. The resulting positions were matched to those stars from the 2MASS catalog. There are hundreds of 2MASS stars within each HST image. By using those 2MASS stars as reference, the astrometric solution yielded root-mean-square residuals of 0.″057 in right ascension (RA) and 0.″065 in declination (Dec) relative to the 2MASS astrometry for the ACS images. The resultant solution gave the residual errors of 0.″068 and 0.″148 in RA and 0.″066 and 0.″149 in Dec relative to the 2MASS astrometry for the PC and WF images, respectively. The final uncertainties of the optical source position in RA and Dec are the root of the square sum of the uncertainty of the astrometry in 2MASS and HST image alignment and the general uncertainties of 2MASS point source astrometry of typically ∼ 0.″1 relative to the ICRS (Skrutskie et al. 2006).

4. Source Identification and Classification

To obtain optical identifications for the X-ray sources we use the precise astrometry described in Section 3. We search for optical counterparts within the 95% Chandra error circle of the source positions (see Table 1 of Elsner et al. 2008), which includes the positional uncertainty of X-ray sources reported by the wavelet source detection algorithm, the uncertainty in the X-ray boresight correction, and the uncertainty in the optical astrometry. Within the half-mass radius of M71, there are 29 sources detected by Chandra and we suggest optical counterparts based on positional coincidence alone to 25 of them. In case of multiple sources inside the X-ray error circle, we include all the candidates. The results of each candidate optical counterpart are summarized in Table 2, and finding charts are shown in Fig. 3 and Fig. 4.

The first step in classifying faint ($L_X \leq 10^{34.5}$ ergs s^{-1}) X-ray sources is to study their X-ray properties, e.g. their X-ray luminosity and spectral behavior (see §2). The second step in the identification process can be made when the sources have other information coming from different wavelengths. The coincidence between accurate radio timing positions of millisecond pulsars and the positions of X-ray sources can provide reliable identification. In the optical band, the color-magnitude diagrams (CMDs) of globular clusters have been studied for a long time because they reflect the fundamental properties of these stars and the evolutionary stage of the globular clusters. We extract further information from the locations of the optical stars in the CMDs of Fig. 2. CVs usually lie much bluer than the main sequence stars in the (V, U–V) and (V, B–V) CMDs while the X-ray ABs may be located on or slightly above the main sequence or on the giant branch. Stars on the main sequence in the V vs. V–I

[6] See http://tdc-www.harvard.edu/software/wcstools/index.html

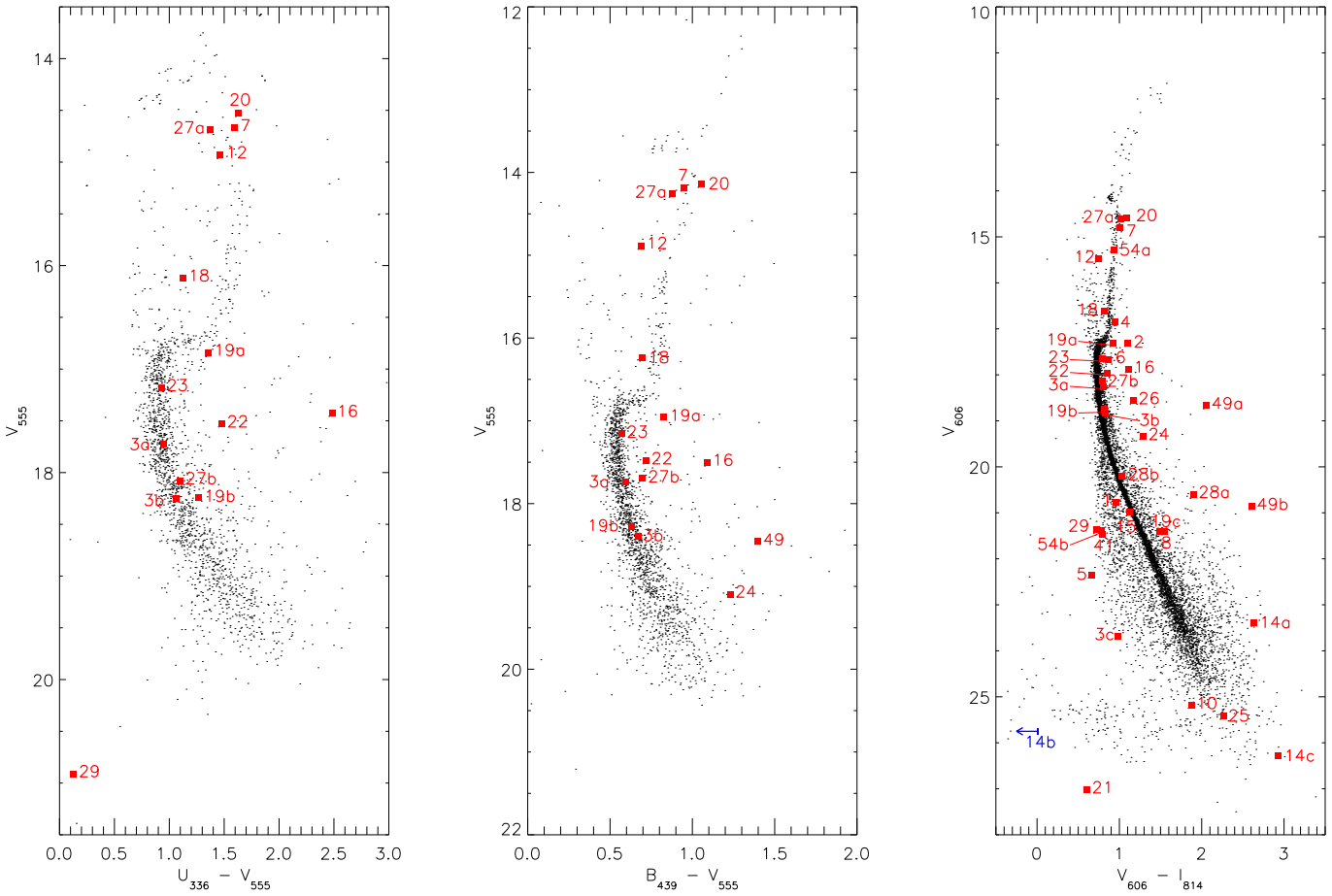

Fig. 2. Color magnitude diagrams (CMDs) for all the sources detected in the WFPC2 and ACS field of view. The HST candidate counterparts matched to the X-ray sources are indicated by red squares. We note here s14b in the (V, V–I) CMD is plotted as a leftward-pointing arrow since its I_{814}-band magnitude is far below the 5-sigma limiting magnitude and with a large magnitude error.

CMD cannot be clearly classified: they could either be CVs or ABs since their optical flux is dominated by the donor stars or brighter stars of the binary systems.

The ratio of X-ray to optical flux is also useful to distinguish CVs from X-ray ABs (see Bassa et al. 2004). In Fig. 5 we show the X-ray luminosity as a function of the absolute magnitude for low-luminosity X-ray sources from 47 Tuc, NGC 6397, NGC 6752, M4, NGC 288, M55, NGC 6366 (data from Grindlay et al. 2001a; Edmonds et al. 2003a; Cool et al. 1998; Grindlay et al. 2001b; Taylor et al. 2001; Pooley et al. 2002; Bassa et al. 2004; Kong et al. 2006; Bassa et al. 2008), and M71. The large symbols in this figure indicate the X-ray sources with possible optical counterparts in the field of view of the Chandra observation of M71, while the smaller symbols show classified objects found in other clusters. We note that the absolute magnitudes and X-ray luminosities for the sources in the observations are computed under the assumption that they are cluster members. As discussed in Elsner et al. (2008), we caution that ~ 40% of the 29 X-ray sources within the half-mass radius are background or foreground objects.

Now we turn to those stars unrelated to the globular clusters. Foreground stars are likely to have counterparts not on the main sequence, have soft spectra, and have low f_X/f_O ratios (Krautter et al. 1999). For background active galactic nuclei (AGN), they will also have counterparts not on the main sequence, but with hard spectra; their f_X/f_O ratios can be high (Krautter et al. 1999). However, the AGN won't necessarily be detected at all; in some cases, the only object in an error circle may be a cluster main-sequence star that is not related to the X-ray source.

We first consider those X-ray sources with only one suggested counterpart in the Chandra error circle. S08 is a known millisecond pulsar, PSR J1953+1846A = M71A, with a spin period of 4.89 ms. It is in a 4.24 hr eclipsing binary system with a low-mass ($\geq 0.032\ M_\odot$) companion. It was discovered with Arecibo (Ransom et al. 2003, 2005; Hessels et al. 2007) and its radio emission is partially eclipsed in the orbital phase interval 0.18 – 0.36 for approximately 20% of each orbit (Hessels et al. 2007). The X-ray counterpart was detected by Elsner et al. (2008). Within the Chandra error circle we find a possible optical counterpart of this pulsar in the V_{606} and I_{814} band. The candidate optical counterpart to s08 lies on the main sequence in our V-I CMD with an absolute magnitude $M_V \sim 8.5$, which implies that it has a mass of about $0.5\ M_\odot$. The radio timing indicates a minimum mass of $0.03\ M_\odot$ (Hessels et al. 2007) for the companion star. In order to allow for such a massive companion (i.e. $\sim 0.5\ M_\odot$), conceivably the orbit could be seen nearly face-on (within 4 degrees). However, in that (extremely unlikely) case we do not expect regular radio eclipses, as are observed. M71A's radio properties are very similar to those of other

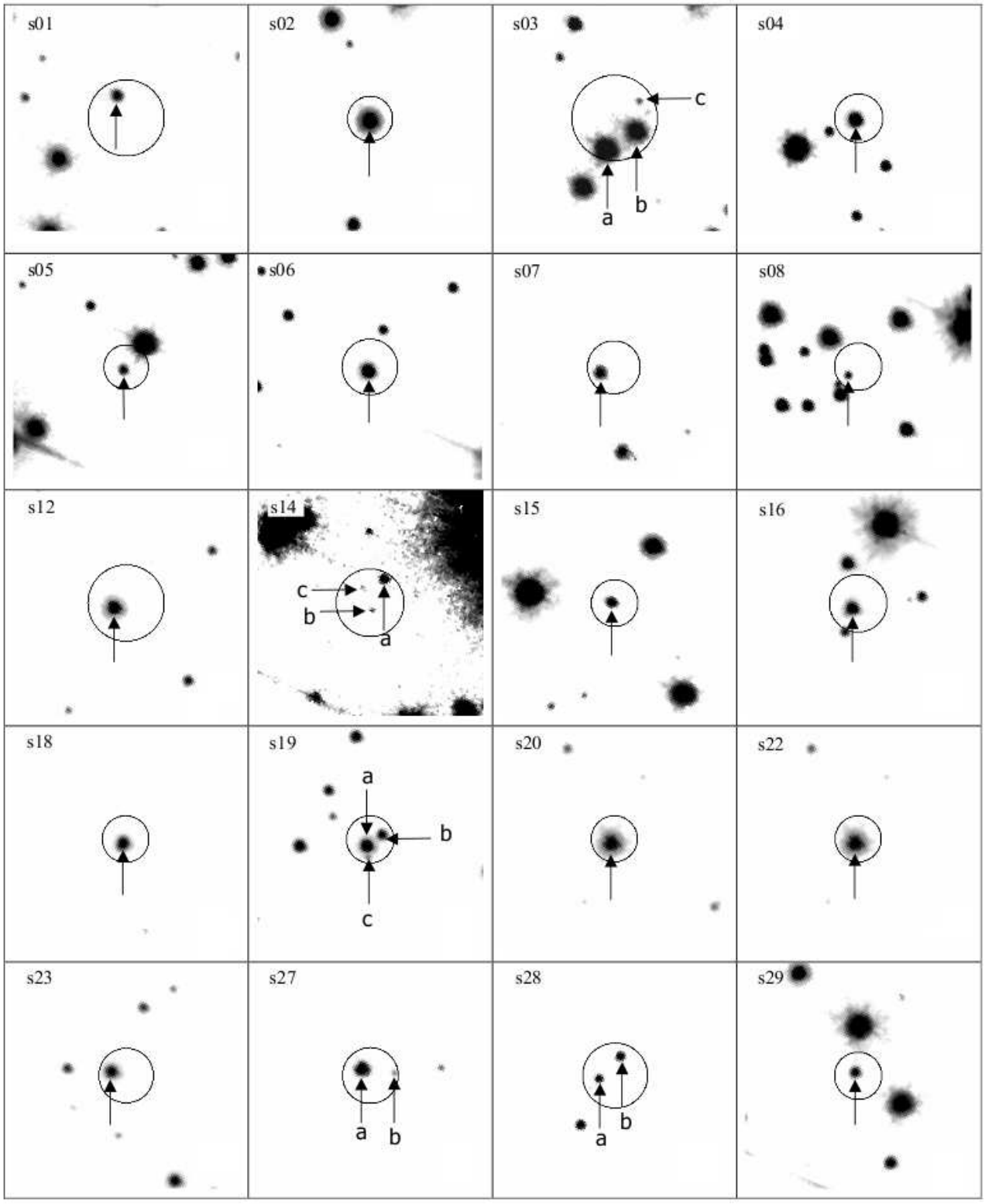

Fig. 3. $5'' \times 5''$ finding charts for candidate optical counterparts within the half-mass radius of M71. The finding charts are obtained from the HST/ACS V_{606} images. The 95% confidence uncertainties on the Chandra positions are overlaid on these charts, while the candidate counterparts are indicated with an arrow. The finding charts are set with their dynamic range. The greyscale of these images is chosen to enhance the visibility of the candidate counterparts. All images have North to the top and East to the left.

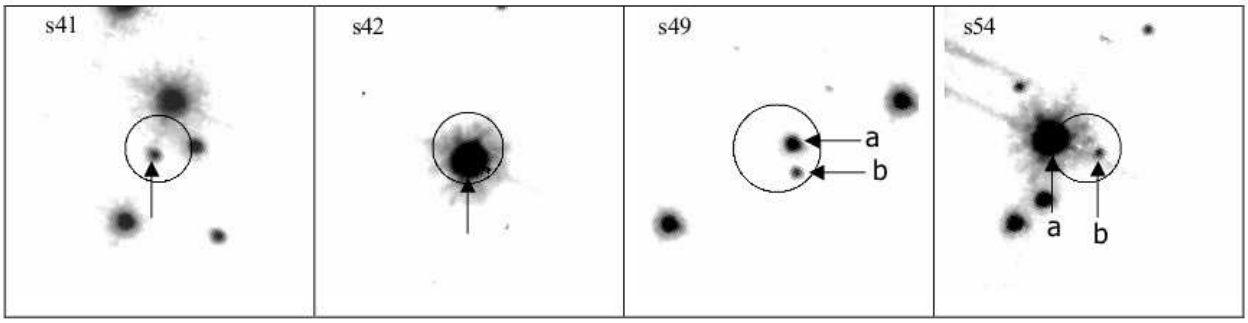

Fig. 4. $5'' \times 5''$ finding charts for candidate optical counterparts outside the half-mass radius of M71. The finding charts are obtained from the HST/ACS V_{606} images. The 95% confidence uncertainties on the Chandra positions are overlaid on these charts, while the candidate counterparts are indicated with an arrow. The finding charts are set with their dynamic range. The greyscale of these images is chosen to enhance the visibility of the candidate counterparts. All images have North to the top and East to the left.

very low-mass binary pulsars such as PSR J1701–3006E (M62E, Freire 2005), and therefore we conclude that M71A's companion is not this star. Although this star's position agrees within 0.″1 with M71A's position from radio timing (I. Stairs 2009, private comm.), transferred with 0.″1 accuracy (1σ) onto the 2MASS frame (Skrutskie et al. 2006), this could be coincidence due to the crowding in this field (Fig. 3); alternatively, M71A could be a hierarchical triple system. Future radio timing may determine this.

The star in the error circle of s02 is nearly located on the main-sequence turn-off point (MSTO) in the (V, V–I) CMD of Fig. 2 and slightly below the subgiant branch, which is similar to the "red straggler" active binaries seen as X-ray sources in other clusters (Albrow et al. 2001; Edmonds et al. 2003a,b; Bassa et al. 2008). Its ratio of the X-ray to optical flux locates in the region of ABs in Fig. 5. Since s02 has a soft spectrum and shows significant time variability in the X-ray band (Elsner et al. 2008) we suggest that s02 is a chromospherically AB and its temporal variation can be explained as flaring on the coronally active star. S04 and s18 are also believed to be in the same group as ABs since both of them are located slightly above the main-sequence turn-off point, have soft X-ray spectra, and have lower X-ray to optical flux ratios.

S05 is the brightest X-ray source within the half-mass radius of M71. It is worth noting that s05 is the only X-ray source detected with ROSAT (Panzera et al. 2003; Elsner et al. 2008) inside the half-mass radius. Its optical counterpart is bluer than the main-sequence, and it has a relatively high X-ray luminosity ($L_{\rm X} \sim 4 \times 10^{31}$ ergs s^{-1}). It is unlikely to be an AB. Its X-ray spectrum is too hard to consider it as a quiescent low-mass X-ray binary (qLMXB). S05 gives a bremsstrahlung temperature consistent with ~ 10 keV, as appropriate for luminous magnetic CVs (Eracleous et al. 1991; Mukai 2003). During the 52.4 ks observation time, it is not consistent with being steady at 99.9% confidence. We suggest that a CV interpretation is plausible. In addition, s05 has a high value of $\log(f_{\rm X}/f_{\rm O}) \sim 0.37$ and the blue color, which implies this source could be a background AGN. However, the power-law fit of its X-ray spectrum, with photon index $\Gamma = 1.55 \pm 0.1$, might be considered as arising from the intra-binary shock formed due to interaction between the relativistic pulsar wind and material from its companion star. An irradiated main-sequence companion could be this blue; e.g. 47 Tuc W (Bogdanov et al. 2005). MSPs with main-sequence companions of the mass of $\sim 0.5 M_{\odot}$ have not yet been detected, but may well be hidden from radio detection by clouds of ionized gas from the companion (e.g. Freire et al. 2004). Therefore, we cannot rule out the interpretation that it is a binary MSP system though this unusual scenario must be judged unlikely.

The candidate cluster counterpart to s29 has ultraviolet excess with respect to the main sequence (Fig. 2) and has a high X-ray to optical flux ratio. The source can be well fitted with a power-law model with a photon index of $\Gamma = 1.29 \pm 0.4$, and its X-ray luminosity is $L_{\rm X,0.3-8.0\ keV} \sim 2.1 \times 10^{31}$ ergs s^{-1}. Its U–V color is far too blue to be an AB while the optical color is redder, almost on the main sequence. That indicates s29 is a CV with two spectral components, a blue disk and a red companion star.

Source s15 is a good AB candidate since there is no evidence for a blue color in the VI CMD and it has a soft X-ray spectrum ($f_{0.5-2.0\ \rm keV}/f_{2.0-6.0\ \rm keV} \geq 1$). On the other hand, without the information from the U–V or B–V color, a CV interpretation is still plausible. Its relatively high value of $\log(f_{\rm X}/f_{\rm O}) \sim -0.79$ suggests that s15 could be a CV, although it doesn't rule out an AB.

The star in the error circle of s20 lies on the giant branch and has a soft X-ray spectrum, which gives strong evidence that it is a chromospherically active binary containing a giant star (i.e., a RS CVn system). Its temporal variation in the X-ray band (Elsner et al. 2008) can be explained by magnetic activity. Since s07 and s12 are located on the giant branch and have relatively low X-ray to optical flux ratios, we believe that they are likely RS CVn systems as well.

The optical counterparts associated with those X-ray sources having lower photon statistics, s01, s06, and s23, are located on the main-sequence and have lower X-ray to optical flux ratios. We then consider that all of them may be X-ray ABs. S22 exhibits rather interesting colors. In the V–I CMD it is on the main sequence, but as we shift to progressively bluer colors its color gets redder and redder while in the U–V CMD it is way off the main sequence. Thus we suggest that it is either a foreground or background source, not associated with M71.

We turn now to the sources with more than one possible counterpart in the error circle. We find two or three possible optical counterparts within each of the Chandra error circles for s03, s14, s19, s27, and s28. S03a and s03b both fall on the main-sequence in the (V, U–V), (V, B–V), and (V, V–I) CMDs. Their

Table 2. Optical counterparts to Chandra X-ray sources within the HST/ACS field of view

X-ray	Offset From CXO position[a]		U_{336}	B_{439}	V_{555}	V_{606}	I_{814}	$\log(L_X)$[b]	$\log(f_X/f_O)$[c]	FAP[d]	Classification[e]
Source	ΔRA (″)	ΔDec (″)	(mag)	(mag)	(mag)	(mag)	(mag)	ergs s^{-1}			
Inside the half-mass radius											
s01	0.22	0.49	…[f]	…	…	20.85(0)	19.94(2)	29.85	-2.02	26.06	AB?
s02	0.0	-0.05	…	…	…	17.38(1)	16.32(1)	31.18	-2.08	1.08	AB
s03a	0.18	-0.69	18.68(6)	18.35(4)	17.78(4)	18.33(1)	17.56(0)	29.95	-2.93	7.01	AB?
s03b	-0.50	-0.29	19.32(9)	19.09(4)	18.44(4)	18.90(1)	18.11(0)	29.95	-2.70	10.36	AB?
s03c	-0.57	0.37	x[g]	x	x	23.8(1)	22.81(6)	29.95	-0.76	37.35	CV/AGN?
s04	0.07	-0.02	…	…	…	16.92(1)	16.01(1)	30.63	-2.82	0.73	AB?
s05	0.06	-0.05	…	…	…	22.42(5)	21.79(0)	31.61	0.37	11.98	CV/AGN?
s06	0.04	-0.08	…	…	…	17.74(1)	16.91(1)	30.15	-2.96	2.67	AB?
s07	0.33	-0.11	16.26(2)	15.16(5)	14.30(5)	14.86(0)	13.89(0)	30.31	-3.96	0.25	AB?
s08	0.24	-0.17	x	x	x	21.48(2)	19.96(1)	30.78	-0.84	11.31	MSP
s10	0.27	0.05	x	x	x	25.25(6)	23.4(1)	30.37	0.26	21.96	CV/AGN?
s12	0.28	-0.10	16.40(2)	15.60(3)	14.93(3)	15.55(0)	14.82(0)	29.88	-4.11	0.72	AB?
s14a	-0.29	0.54	x	x	x	23.47(6)	20.87(2)	30.03	-0.80	33.60	F?
s14b	-0.04	-0.18	x	x	x	25.8(1)	28(2)	30.03	0.12	48.35	CV/AGN?
s14c	0.18	0.36	x	x	x	26.4(2)	23.46(6)	30.03	0.36	51.13	CV/AGN?
s15	0.10	0.06	…	…	…	21.06(6)	19.98(4)	31.0	-0.79	10.37	CV/AB?
s16	0.15	-0.09	19.9(1)	18.62(4)	17.55(3)	17.95(1)	16.88(0)	30.15	-2.88	3.44	F?
s18	0.08	-0.08	17.25(3)	16.96(6)	16.28(6)	16.69(1)	15.92(1)	30.77	-2.77	0.58	AB
s19a	0.08	-0.12	18.20(5)	17.79(3)	16.99(3)	17.39(0)	16.50(0)	30.95	-2.30	1.16	AB?
s19b	-0.28	0.10	19.52(9)	18.93(4)	18.32(4)	18.83(1)	18.05(1)	30.95	-1.73	4.62	AB?
s19c	0.18	0.36	x	x	x	21.48(1)	20.04(2)	30.95	-0.66	11.33	AB?
s20	0.08	-0.07	16.16(2)	15.21(3)	14.18(4)	14.65(0)	13.61(0)	31.18	-3.17	0.16	AB
s21	0.17	-0.15	x	x	x	27.09(9)	26.5(3)	29.99	0.61	42.03	CV/AGN?
s22	0.14	-0.15	19.01(7)	18.22(5)	17.52(3)	18.03(0)	17.22(1)	30.02	-2.98	5.48	F?
s23	0.32	0.09	18.11(5)	17.75(3)	17.19(3)	17.73(1)	16.73(1)	30.22	-2.91	2.49	AB?
s24	0.21	0.05	x	20.3(1)	19.13(4)	19.4(1)	18.16(1)	30.02	-2.43	9.81	F
s25	0.08	0.06	x	x	x	25.49(8)	23.3(1)	30.03	0.01	30.34	CV/AGN?
s26	-0.07	-0.08	…	19.3(2)	18.33(7)	18.63(7)	17.50(3)	30.66	-2.10	4.88	F
s27a	0.19	0.17	16.06(2)	15.15(4)	14.23(4)	14.68(0)	13.70(0)	30.22	-4.12	0.24	AB?
s27b	-0.57	0.06	19.18(8)	18.41(3)	17.73(3)	18.19(1)	17.45(1)	30.22	-2.72	4.09	AB?
s28a	0.35	-0.06	x	…	…	20.67(0)	18.81(0)	29.99	-1.96	17.96	F?
s28b	-0.15	0.44	x	…	…	20.28(1)	19.28(1)	29.99	-2.11	16.12	AB?
s29	0.05	0.06	21.0(2)	…	20.9(2)	21.44(1)	20.76(1)	30.85	-0.79	11.20	CV
Outside the half-mass radius											
s41	0.13	-0.12	…	…	…	21.53(1)	20.77(1)	30.69	-0.91	14.47	CV/AGN?
s49a	-0.24	0.09	…	19.87(7)	18.49(3)	18.74(1)	16.72(1)	30.13	-2.59	9.43	F
s49b	-0.31	-0.38	…	x	x	20.93(2)	18.35(1)	30.12	-1.71	21.64	F
s54a	0.68	0.20	…	…	…	15.36(0)	14.46(0)	30.62	-3.45	0.65[h]	AB?
s54b	-0.23	-0.05	…	…	…	21.46(1)	20.72(1)	30.62	-1.01	19.76[h]	CV/AGN?

[a] The position offsets of sources detected in the V_{606} band are given relative to their Chandra positions (see Elsner et al. 2008 for details)

[b] L_X: unabsorbed X-ray luminosity in the energy band is 0.5–2.5 keV (see Table 5 of Elsner et al. 2008)

[c] Ratio of X-ray to optical (V_{606}) flux is computed by using $\log(f_X/f_O) = \log f_X + 0.4V_{606} + 5.07$; f_X is derived in the 0.5–2.5 keV band.

[d] FAP: False Alarm Probability (%). The probability of a chance coincidence in % is calculated from $P_{coinc} = N(< m)\pi r_{95}^2/A_{search}$ (see §6.1 of Elsner et al. 2008). The search area, A_{search}, is the central region of M71 with the radius of 2′ (see Anderson et al. 2008) and the considered magnitude, m, is V_{606} band magnitude.

[e] MSP: millisecond pulsar; CV: cataclysmic variable; AB: X-ray active binary; AGN: active galactic nucleus; F: foreground source; ?: all cases where we are not certain about the nature of the X-ray source.

[f] Sources lying outside the field-of-view of the WFPC2 chips do not have F336W, F439W or F555W data

[g] Under detection limit.

[h] Since the source is outside the searching region of the 2′-radius central circle (Anderson et al. 2008), the A_{search} for the probability of a chance coincidence is calculated with the HST/ACS field of view, i.e. 202″ × 202″.

colors and low X-ray to optical flux ratios suggest that either s03a or s03b is a chromospherically AB. However, the blue color and the relatively high X-ray to optical flux ratio of s03c indicates that it is a CV or a background AGN. S14a and s28a are located far from the main sequence, suggesting that they do not belong to M71, while s28b located on the main sequence could be an active binary system since it has the relatively low X-ray to optical flux ratio. In Fig. 3, we find two additional possible optical counterparts, s14b and s14c, within the Chandra error circle of s14, which are fainter than the 5-σ limiting magnitudes of V_{606} and I_{814}. Based on the blue color and the high value of f_X/f_O, s14b could be either a CV or a background AGN. The optical-faint source s14c is located near the downward-extended part of the main sequence, suggesting that it could be a main-sequence star. However, it is located in the L_X vs. M_V diagram in a region where no authentic cluster members have been found

if we compute its X-ray luminosity and absolute magnitude under the assumption that it belongs to M71. We then rule out the AB interpretation. Therefore, due to its high X-ray to optical flux ratio of this source, s14c is considered as either a good candidate for background AGN with a optically faint object inside the error circle not related to the X-ray source or a CV candidate with a secondary star that dominates the optical flux in the (V, V–I) CMD. There are three optical counterparts within the Chandra error circle of s19. The position of s19a is near the MSTO point and slightly below the subgiant branch, which is similar to the case of s02, while s19b is located on the main sequence. Both of their X-ray to optical flux ratios are located in the region that is primarily populated by ABs (Fig. 5). For the third optical counterpart, s19c, its location in the VI CMD and soft X-ray spectrum indicate that s19c is an active binary as well. However, without the information from the UV color we cannot eliminate the CV interpretation due to its relatively high X-ray to optical flux ratio, which is similar to the case of s15. We suggest that s19a is the most likely counterpart, as red stragglers are very often associated with X-ray sources (e.g. Heinke et al. 2005). According to the positions of two possible optical counterparts to s27 in the CMDs and in the absolute magnitude vs. X-ray luminosity diagram, we believe that either s27a or s27b is likely to be an active binary.

The optical counterparts of s16, s24, and s26 are located further above or to the right of the main sequence than the binary sequence. Hence we believe that they are foreground objects and unrelated to M71. The positions of two faint optical counterparts to s10 and s25 in the (V, V–I) CMD and their relatively high X-ray to optical flux ratios are very similar to the case of s14c so that s10 and s25 could be either CVs or background AGN. The highest X-ray to optical flux ratio among 39 possible counterparts and blue color suggests that s21 is the most likely background AGN although we cannot eliminate the interpretation of a CV. Furthermore, the regions of the X-ray sources, s09, s11, s13, and s17, were also observed with the HST/WFPC2 and ACS, but we do not find any optical counterparts inside their Chandra error circles. If we set the 5-σ limiting magnitude of $V_{606} = 25.17$ as the upper limit for these sources, their X-ray to optical flux ratios fall on a range of ~ 0.2–0.6, which are higher than the highest $\log(f_X/f_O)$ value known for an AB in a cluster, e.g. W64 in 47 Tuc (Edmonds et al. 2003a). Therefore, an AB interpretation can be rejected. If we take their X-ray colors into account, s11 and s17 are located near the bottom-right corner and close to the position of s40 in the X-ray color-color diagram shown in Fig. 4 of Elsner et al. (2008), which implies they have very hard spectra with over half of their counts above 2 keV. This infers a high intrinsic N_H, which strongly suggests that these are background AGN. For the other three sources with medium X-ray colors, we then tentatively classify them all as CVs, MSPs, or background AGN, though AGN are probably the most likely category.

Outside the half-mass radius of M71, we find 6 optical counterparts to X-ray sources, s41, s42, s49 and s54 in the ACS field-of-view. The candidate counterpart to s42, located on the edge of the ACS, is saturated in the optical band, which prevents us from obtaining a reliable magnitude of this optical source or searching for any other faint optical sources inside the Chandra error circle. There are 2 possible optical counterparts to s49. Both of them are located far from the main sequence, hence we suggest that they are not associated with M71. Inside the error circle of s54, the brighter object s54a is on the giant branch while the fainter one, s54b, is located blueward of the main sequence in the CMD and has a relatively high X-ray to optical flux ratio,

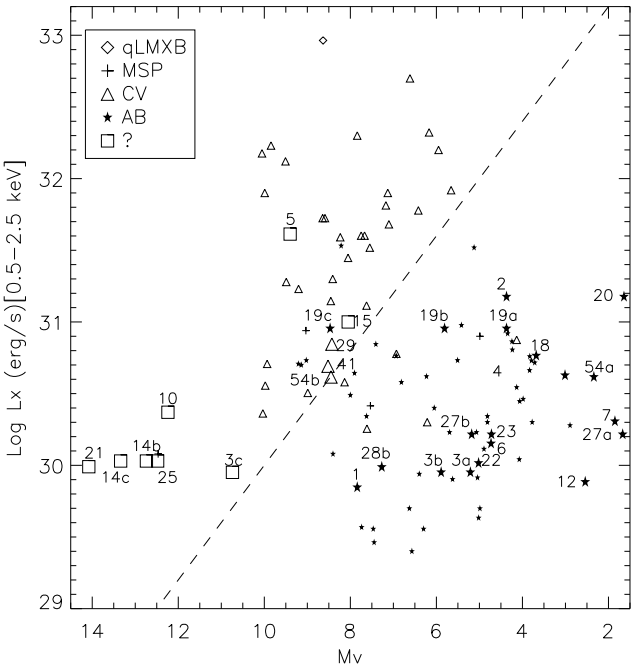

Fig. 5. X-ray luminosity as a function of absolute magnitude, for low-luminosity X-ray sources in globular clusters. Five types of X-ray sources are shown, qLMXBs (diamonds), MSPs (crosses), CVs (triangles), ABs (stars), and unclassified sources (squares). The larger and numbered symbols in this figure correspond to the optically identified X-ray sources in the field of view of the Chandra observation of M71, where we compute absolute magnitude and X-ray luminosity under the assumption that the sources are associated with M71. The smaller symbols in this figure indicate objects found in other clusters, i.e. 47 Tuc, NGC 6397, NGC 6752, M4, NGC 288, M55, and NGC 6366. We note that ambiguous sources coming from other clusters were discarded in this figure. The dashed line of constant X-ray to optical flux ratio given by $\log L_{X,0.5-2.5\ \mathrm{keV}}(\mathrm{ergs\ s^{-1}}) = 34.0 - 0.4\ M_V$ (after Bassa et al. 2004) roughly separates CVs from ABs.

suggesting that s54b might be a CV. However, s54b lies on the spikes produced by s54a, which prevents us from obtaining an accurate magnitude for s54b. S41's color is bluer than the main sequence, and its X-ray to optical flux ratio is higher than that of an AB. We then suggest that s41 is a CV candidate. Furthermore, a background AGN scenario is also plausible for s41 and s54b due to their blue colors, high $\log(f_X/f_O)$ values, and their locations outside the half-mass radius of M71, where they are more likely to be background sources.

5. Summary and Discussion

In summary, we find one certain CV (s29), seven possible candidate CVs (s05, s10, s14, s21, s25, s41, and s54), and two certain ABs (s02 and s20) and 12 good candidate ABs (s01, s03, s04, s06, s07, s12, s15, s18, s19, s23, s27, and s28) in the globular cluster M71. Some of our candidate CVs (and/or candidate ABs) might be MSPs in binary systems or AGN, which often (but not always) show blue colors.

To interpret our results, understanding how many of our objects are likely false matches will be critical. We calculated the expected number of false matches in several ways. First, we

shifted all our X-ray source positions by 9″ and 18″ (somewhat arbitrary, but chosen to be larger than the largest uncertainties) in four directions, and searched for matches against the V_{606} frame. From this exercise, we expect 11^{+4}_{-8} false matches among our 39 possible matches, indicating that $\gtrsim$ 70% of the 34 total X-ray sources in our field of view have a true match. By chance, then, 70% of our false matches should occur with sources which have a true match—suggesting that $\sim$ 7.7 sources should have two possible optical counterparts. We see seven sources that have two or more possible V_{606} counterparts, which is nicely consistent.

In order to know which sources are more likely to have false matches, we calculated the probability of a chance coincidence in % shown in Col. 10 of Table 2 by using Eq. (3) from Elsner et al. (2008) (see also Verbunt et al. 2008). Within the half-mass radius, there are 6 sources with a false alarm probability smaller than 1%, which indicates that those associations between X-ray sources and optical counterparts have a >99% confidence level. Adding up the false alarm probabilities gives a total expected number of false matches of $\sim$ 5, which is consistent with the the expectation of 11^{+4}_{-8} false matches above. Among the 10 X-ray sources with optical counterparts and $L_{\rm X,0.5-6.0\ keV} > 4\times10^{30}$ ergs s^{-1}, adding the false alarm probabilities indicates that roughly one of them is expected to be a false match. (Note that we believe s08 to be a false match, but to be a true cluster member; and that s19 has three potential counterparts.)

Inside the half-mass radius of M71, we find 14 X-ray sources with $L_{\rm X,0.5-6.0\ keV} > 4\times10^{30}$ ergs s^{-1}, of which 10 have optical counterparts. Assuming that all X-ray sources outside the half-mass radius are fore- or background sources, we can estimate that $\sim 3.7^{+3.1}_{-1.8}$ X-ray sources among 14 are unrelated to M71. The error quote here is from the Poisson statistic (Gehrels 1986). This is consistent with our estimate above that we have identified true optical counterparts for $\sim$ 9 X-ray sources.

Pooley et al. (2003) have shown that for 12 globular clusters observed by Chandra, the number of globular cluster X-ray sources which are above the lower limit of 4×10^{30} ergs s^{-1} (0.5–6 keV) can be approximately linearly fitted with the predicted stellar encounter rate $\Gamma' \propto {\rho_o}^{1.5} {r_c}^2 \equiv \Gamma$, where Γ is referred to as the collision number (Verbunt 2003). Here ρ_o is the central density of the cluster, and $r_{\rm c}$ is the core radius. In order to examine if M71 fits this relation we compare its number of X-ray sources and its collision number Γ with those of some other clusters, NGC 6266, 47 Tuc, M28, M4, NGC 6366, M55, and NGC 288 (see Fig. 6), using the parameters listed in Table 3. We note that the core-collapsed globular clusters are not considered in our study since their core parameters are generally uncertain, introducing strong uncertainties into interaction rates derived from those parameters. The encounter number for M71 is $\sim$ 230 and $\sim$ 10 times smaller than those of 47 Tuc and M4, respectively. Pooley et al. (2003) reports 41±2 sources above the lower luminosity limit in 47 Tuc, which are revised by Heinke et al. (2005) to 63±4 (for a distance of 4.5 kpc); the uncertainty is due to the estimated number of background sources. Thus, if the number of sources scales with the encounter rate, the presence of $\sim 10 \pm 3$ sources with $L_{\rm X,0.5-6.0\ keV} > 4\times10^{30}$ ergs s^{-1} in M71 is a very significant overabundance, even if we take into account the errors due to Poissonian fluctuations. The same conclusion is reached on the basis of comparison with any other globular clusters listed in Table 3 except for M55 and NGC 288, in which the number of the X-ray sources is also in excess of the predicted value. This indicates that most of the sources in M71, M55, and NGC 288 are not formed via stellar encounters.

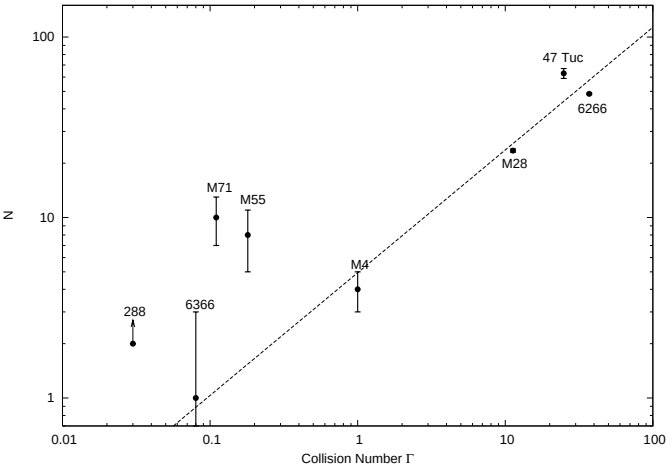

Fig. 6. Number of globular cluster X-ray sources (N) with $L_{\rm X,0.5-6.0\ keV} \geq 4\times10^{30}$ ergs s^{-1} inside the half-mass radius vs. the normalized collision number Γ of the cluster. The dashed line indicates the best power-law fit of the data points from 47 Tuc, NGC 6266, M28, M4, and NGC 6366 (cf. Table 3). The relation between N and Γ, i.e. $N \propto \Gamma^{0.74\pm0.03}$, is consistent with the result derived from Pooley et al. (2003).

As suggested by Verbunt (2002), ABs are most likely primordial binaries, and thus to first order their numbers should scale with mass. Following Kong et al. (2006), we calculated the half masses with $10^{-0.4M_V}$, assuming the visual mass-to-light ratio is the same for all clusters listed in Table 3. M71 has the lowest half-mass, containing only $\sim$ 30% of the mass within the half-mass radius of M 4. Scaled by mass, the predicted number of ABs with $L_{\rm X,0.5-6\ keV} > 4\times10^{30}$ ergs s^{-1} in M 71 should be similar to that of NGC 6366 and smaller than those in any other cluster shown in Table 3, but this is in contrast to our results.

The scaling of source number with the collision number for the sources with $L_{\rm X,0.5-6\ keV} > 4\times10^{30}$ ergs s^{-1} suggests that CVs are mostly made via stellar encounters (Pooley et al. 2003). If we assumed that all of the CVs in M71 were formed dynamically, we would not expect to find more than one CV by scaling with the encounter numbers from any other cluster listed in Table 3. However, most of the globular clusters studied by Pooley et al. (2003) have high Γ numbers and many dynamically produced CVs. It is reasonable to suspect that primordial CVs may dominate in the low-density clusters. According to the computations by Davies (1997), a cluster core with a star density of 1000 pc^{-3} allows most of the CV progenitors to evolve into a CV. This could explain the existence of at least one (and several candidate) CVs within the half-mass radius of M71.

It is interesting to mention that in M71 $\sim$7 optical counterparts to Chandra X-ray sources are classified as potential RS CVn systems, in which X-ray emission is produced primarily in (sub)giant flare outbursts. A couple possible RS CVn X-ray sources have been identified in 47 Tuc (Heinke et al. 2005) and ω Centauri (Cool et al. 2002), but, besides M71, only the low-density clusters M55 and NGC 6366 (Bassa et al. 2008) have significant fractions of X-ray sources identified as possible RS CVns. Considering the even lower density case, the total X-ray luminosity of the old open cluster M 67 is dominated by binaries with giants (van den Berg et al. 2004). From the ROSAT census, the X-ray emission of most globular clusters per unit mass is lower than that of the old open cluster M67 (Verbunt 2001, 2002). There are three possible explanations for this: a) M67 is

Table 3. Scaling parameters of NGC 6266, 47 Tuc, M28, M4, M71, NGC 6366, M55, and NGC 288

(1) Cluster	(2) $\log \rho_0$ ($L_\odot$pc^{-3})	(3) r_c ($''$)	(4) d (kpc)	(5) M_V	(6) Γ	(7) M_h	(8) Source	(9) Background	(10) Member	(11) IDs.	(12) Reference[a]
NGC 6266	5.14	10.8	6.9	−9.19	37.07	8.24	51	2-3	48-49	2[c]	1,2,3
47 Tuc	4.81	24.0	4.5	−9.4	24.91	10.0	79	∼16	63±4	53-63	4
M 28	4.75	14.4	5.6	−8.33	11.29	3.73	26	2-3	23-24	2[c]	1,5,6
M 4	4.01	49.8	1.73	−6.9	1.0	1.0	6	1-3	3-5	5	1,7
M 71	3.05	37.8	4.0	−5.6	0.11	0.30	14	1-7	10±3	4-9	8
NGC 6366	2.42	109.8	3.6	−5.77	0.08	0.33	5	2-5	1^{+2}_{-1}	∼1	9
M 55	2.15	169.8	5.3	−7.6	0.18	1.82	16	5-12	8^{+3}_{-4}	2-4	9
NGC 288[b]	1.80	85.0	8.4	−6.7	0.03	0.83	11	4-11	4^{+3}_{-4}	2-5	10

Note: Cols. 2–5 give the values for central density (ρ_0), core-radius (r_c), distance (d) and absolute visual magnitude (M_V) originate from Harris (1996, version of February 2003). For M4, the values of ρ_0 and M_V are computed for the distance and reddening of Richer et al. (1997). Cols. 6 and 7 are the collision number which is computed from $\Gamma \equiv \rho_0^{1.5} r_c^2$ and the half-mass from $M_h \propto 10^{-0.4 M_V}$ (Kong et al. 2006). Values for Γ and M_h are normalized to the value of M4. Col. 8 shows the total number of sources detected within the half-mass radius. Col. 9 is the number of expected fore/background sources. Col. 10 gives the number of expected cluster members plus error. Col. 11 shows the number of X-ray sources (with $L_{X,0.5-6.0\ keV} > 4 \times 10^{30}$ ergs s^{-1}) which have optical or/and radio counterparts associated with the cluster, or spectrally confirmed qLMXBs. The last column gives the reference paper. These globular clusters are ordered on the central density.

a. For each cluster, the basic data for this table were extracted from: 1. Pooley et al. (2003); 2. Cocozza et al. (2008); 3. Trepl (2007); 4. Heinke et al. (2005); 5. Becker et al. (2003); 6. Becker & Hui (2007); 7. Bassa et al. (2004); 8. this work; 9. Bassa et al. (2008); 10. Kong et al. (2006).

b. NGC 288 was not observed long enough to reach this luminosity limit of $L_X \sim 4.0 \times 10^{30}$ ergs s^{-1} in the 0.5–6.0 keV range. Its limiting luminosity is $\sim 5.7 \times 10^{30}$ ergs s^{-1}. However, we keep this cluster's data, as a lower limit, since we have so few constraints on low-density clusters.

c. No information about the optical counterparts to X-ray sources.

a very sparse cluster, which is evaporating its lowest-mass stars (Hurley et al. 2005). Open clusters don't survive very long. As a cluster evaporates its lowest-mass stars, it tends to retain its heaviest systems–binaries–which are more likely to be X-ray sources. b) M67 is a rather young cluster. Younger stars may produce more X-rays (Randich 1997), since they tend to be rotating faster than older stars. c) A large fraction of binary systems are destroyed in globular clusters (see Ivanova et al. 2005), in particular those with longer orbits. RS CVn systems involve giants that are spun up by stellar companions. These systems must be relatively wide binaries, in order to avoid the giant swallowing its companion as it evolves; but such wide binaries are destroyed in globular clusters. Thus there are fewer RS CVn binaries in globulars. Since RS CVn binaries tend to be brighter than BY Dra binaries (main-sequence ABs), low-density clusters can have startlingly high X-ray luminosities per unit mass.

To summarize the results of this paper, the number of X-ray faint sources with $L_{X,0.5-6\ keV} > 4 \times 10^{30}$ ergs s^{-1} found in M71 is higher than the predicted value on the basis of either the collision frequency or the half mass. We suggest that those CVs and ABs in M71 are primordial in origin. The last interpretation above may explain the X-ray overabundance of low-density clusters like M 71, where fewer primordial binaries may have been destroyed through binary interactions. Study of other low-density globular clusters will help us to better understand their evolution and dynamics.

Acknowledgements. This work made use of the Chandra and HST data archives. We acknowledge that Stairs et al. kindly provide us the information of M71A in advance of publication. We also thank Anderson et al. for the photometry. The first author thanks Albert K.H. Kong for providing some helpful suggestions and acknowledges the receipt of funding provided by the Max-Planck Society in the frame of the International Max-Planck Research School (IMPRS). COH acknowledges support from NASA Chandra grants, and funding from NSERC and the University of Alberta.

References

Albrow, M. D., Gilliland, R. L., Brown, T. M., et al. 2001, ApJ, 559, 1060
Aldcroft, T. L., Karovska, M., Cresitello-Dittmar, M. L., Cameron, R. A., & Markevitch, M. L. 2000, in Presented at the Society of Photo-Optical Instrumentation Engineers (SPIE) Conference, Vol. 4012, Proc. SPIE Vol. 4012, p. 650-657, X-Ray Optics, Instruments, and Missions III, Joachim E. Truemper; Bernd Aschenbach; Eds., ed. J. E. Truemper & B. Aschenbach, 650–657
Anderson, J., Sarajedini, A., Bedin, L. R., et al. 2008, AJ, 135, 2055
Ashman, K. M. & Zepf, S. E. 1998, Globular cluster systems (Cambridge University Press)
Bassa, C., Pooley, D., Homer, L., et al. 2004, ApJ, 609, 755
Bassa, C. G., Pooley, D., Verbunt, F., et al. 2008, A&A, 488, 921
Becker, W. & Hui, C. Y. 2007, astro-ph/07050119
Becker, W., Swartz, D. A., Pavlov, G. G., et al. 2003, ApJ, 594, 798
Bogdanov, S., Grindlay, J. E., & van den Berg, M. 2005, ApJ, 630, 1029
Cash, W. 1979, ApJ, 228, 939
Cocozza, G., Ferraro, F. R., Possenti, A., et al. 2008, ApJ, 679, L105
Cool, A. M., Grindlay, J. E., Cohn, H. N., Lugger, P. M., & Bailyn, C. D. 1998, ApJ, 508, L75
Cool, A. M., Haggard, D., & Carlin, J. L. 2002, in Astronomical Society of the Pacific Conference Series, Vol. 265, Omega Centauri, A Unique Window into Astrophysics, ed. F. van Leeuwen, J. D. Hughes, & G. Piotto, 277
Davies, M. B. 1997, MNRAS, 288, 117
Dolphin, A. E. 2000, PASP, 112, 1397
Edmonds, P. D., Gilliland, R. L., Heinke, C. O., & Grindlay, J. E. 2003a, ApJ, 596, 1177
Edmonds, P. D., Gilliland, R. L., Heinke, C. O., & Grindlay, J. E. 2003b, ApJ, 596, 1197
Elsner, R. F., Heinke, C. O., Cohn, H. N., et al. 2008, ApJ, 687, 1019
Eracleous, M., Halpern, J., & Patterson, J. 1991, ApJ, 382, 290
Ferraro, F. R., Paltrinieri, B., Rood, R. T., Fusi Pecci, F., & Buonanno, R. 2000, ApJ, 537, 312
Freire, P. C., Gupta, Y., Ransom, S. M., & Ishwara-Chandra, C. H. 2004, ApJ, 606, L53
Freire, P. C. C. 2005, in Astronomical Society of the Pacific Conference Series, Vol. 328, Binary Radio Pulsars, ed. F. A. Rasio & I. H. Stairs, 405
Gehrels, N. 1986, ApJ, 303, 336
Grindlay, J. E., Heinke, C., Edmonds, P. D., & Murray, S. S. 2001a, Science, 292, 2290
Grindlay, J. E., Heinke, C. O., Edmonds, P. D., Murray, S. S., & Cool, A. M. 2001b, ApJ, 563, L53
Grindlay, J. E., Hertz, P., Steiner, J. E., Murray, S. S., & Lightman, A. P. 1984, ApJ, 282, L13
Harris, W. E. 1996, AJ, 112, 1487
Heinke, C. O., Grindlay, J. E., Edmonds, P. D., et al. 2005, ApJ, 625, 796

Hessels, J. W. T., Ransom, S. M., Stairs, I. H., Kaspi, V. M., & Freire, P. C. C. 2007, ApJ, 670, 363
Heyer, I., Biretta, J., Brammer, G., et al. 2004, WFPC2 Instrument Handbook, Version 9.0 (Baltimore: STScI).
Holtzman, J. A., Burrows, C. J., Casertano, S., et al. 1995, PASP, 107, 1065
Hurley, J. R., Pols, O. R., Aarseth, S. J., & Tout, C. A. 2005, MNRAS, 363, 293
Ivanova, N., Fregeau, J. M., & Rasio, F. A. 2005, in Astronomical Society of the Pacific Conference Series, Vol. 328, Binary Radio Pulsars, ed. F. A. Rasio & I. H. Stairs, 231
Koekemoer, A. M., Fruchter, A. S., Hook, R. N., & Hack, W. 2002, in The 2002 HST Calibration Workshop : Hubble after the Installation of the ACS and the NICMOS Cooling System, ed. S. Arribas, A. Koekemoer, & B. Whitmore, 337
Kong, A. K. H., Bassa, C., Pooley, D., et al. 2006, ApJ, 647, 1065
Krautter, J., Zickgraf, F.-J., Appenzeller, I., et al. 1999, A&A, 350, 743
Lugger, P. M., Cohn, H. N., Heinke, C. O., Grindlay, J. E., & Edmonds, P. D. 2007, ApJ, 657, 286
Mukai, K. 2003, Advances in Space Research, 32, 2067
Panzera, M. R., Campana, S., Covino, S., et al. 2003, A&A, 399, 351
Piotto, G., King, I. R., Djorgovski, S. G., et al. 2002, A&A, 391, 945
Pooley, D., Lewin, W. H. G., Anderson, S. F., et al. 2003, ApJ, 591, L131
Pooley, D., Lewin, W. H. G., Homer, L., et al. 2002, ApJ, 569, 405
Predehl, P. & Schmitt, J. H. M. M. 1995, A&A, 293, 889
Randich, S. 1997, Memorie della Societa Astronomica Italiana, 68, 971
Ransom, S., Hessels, J., Stairs, I., et al. 2005, in Astronomical Society of the Pacific Conference Series, Vol. 328, Binary Radio Pulsars, ed. F. A. Rasio & I. H. Stairs, 199
Ransom, S. M., Hessels, J. W. T., Stairs, I. H., et al. 2003, in Astronomical Society of the Pacific Conference Series, Vol. 302, Radio Pulsars, ed. M. Bailes, D. J. Nice, & S. E. Thorsett, 371
Seaton, M. J. 1979, MNRAS, 187, 73P
Sirianni, M., Jee, M. J., Benítez, N., et al. 2005, PASP, 117, 1049
Skrutskie, M. F., Cutri, R. M., Stiening, R., et al. 2006, AJ, 131, 1163
Taylor, J. M., Grindlay, J. E., Edmonds, P. D., & Cool, A. M. 2001, ApJ, 553, L169
Trepl, L. 2007, LMU Diploma Thesis
van den Berg, M., Tagliaferri, G., Belloni, T., & Verbunt, F. 2004, A&A, 418, 509
Verbunt, F. 2001, A&A, 368, 137
Verbunt, F. 2002, in Astronomical Society of the Pacific Conference Series, Vol. 265, Omega Centauri, A Unique Window into Astrophysics, ed. F. van Leeuwen, J. D. Hughes, & G. Piotto, 289
Verbunt, F. 2003, in Astronomical Society of the Pacific Conference Series, Vol. 308, Astronomical Society of the Pacific Conference Series, ed. E. P. van den Heuvel, L. Kaper, E. Rol, & R. A. M. J. Wijers, 201
Verbunt, F. & Lewin, W. H. G. 2004, ArXiv Astrophysics e-prints
Verbunt, F., Pooley, D., & Bassa, C. 2008, in IAU Symposium, Vol. 246, IAU Symposium, 301–310